

Real-time approach to the optical properties of solids and nanostructures: Time-dependent Bethe-Salpeter equation

C. Attaccalite,¹ M. Grüning,^{2,3} and A. Marini^{4,5}¹*Institut Néel, CNRS/UJF, 25 rue des Martyrs BP 166, FR-38042 Grenoble cedex 9, France*²*Centre for Computational Physics and Physics Department, University of Coimbra, Rua Larga, PT-3004-516 Coimbra, Portugal*³*European Theoretical Spectroscopy Facility, NAPS/IMCN, Université Catholique de Louvain, BE-1348 Louvain-la-Neuve, Belgium*⁴*Istituto di Struttura della Materia (ISM), Consiglio Nazionale delle Ricerche, Via Salaria Km 29.5, CP 10, 00016 Monterotondo Stazione, Italy*⁵*Ikerbasque, Basque Foundation for Science, ES-48011 Bilbao, Spain*

(Received 12 September 2011; revised manuscript received 21 November 2011; published 13 December 2011)

Many-body effects are known to play a crucial role in the electronic and optical properties of solids and nanostructures. Nevertheless, the majority of theoretical and numerical approaches able to capture the influence of Coulomb correlations are restricted to the linear response regime. In this work, we introduce an approach based on a real-time solution of the electronic dynamics. The proposed approach reduces to the well-known Bethe-Salpeter equation in the linear limit regime and it makes it possible, at the same time, to investigate correlation effects in nonlinear phenomena. We show the flexibility and numerical stability of the proposed approach by calculating the dielectric constants and the effect of a strong pulse excitation in bulk *h*-BN.

DOI: [10.1103/PhysRevB.84.245110](https://doi.org/10.1103/PhysRevB.84.245110)

PACS number(s): 78.20.Bh, 78.47.je, 73.22.-f

I. INTRODUCTION

Real-time methods have proven their utility in calculating optical properties of finite systems mainly within time-dependent density functional theory (TDDFT).^{1,2} On the other hand, extended systems have been mostly studied by using many-body perturbation theory (MBPT) within the linear response regime.³ The different treatment of correlation and nonlinear effects marks the range of applicability of the two approaches. The real-time TDDFT makes it possible to investigate nonlinear effects such as second harmonic generation⁴ or hyperpolarizabilities of molecular systems.² However, the standard approaches used to approximate the exchange-correlation functional of TDDFT treat correlation effects only on a mean-field level. As a consequence, while finite systems (such as molecules) are well described, in the case of extended systems (such as periodic crystals and nano-structures), the real-time TDDFT does not capture the essential features of the optical absorption⁵ even qualitatively.

On the contrary, MBPT allows us to include correlation effects using controllable and systematic approximations for the self-energy Σ , that is, a one-particle operator nonlocal in space and time. Σ can be evaluated within different approximations, among which one of the most successful is the so-called *GW* approximation.⁶ Since its first application to semiconductors,⁷ the *GW* self-energy has been shown to correctly reproduce quasiparticle energies and lifetimes for a wide range of materials.⁶ Furthermore, by using the static limit of the *GW* self-energy as scattering potential of the Bethe-Salpeter equation (BSE),³ it is possible to calculate response functions including electron-hole interaction effects.

In recent years, the MBPT approach has been merged with density functional theory (DFT) by using the Kohn-Sham Hamiltonian as zeroth-order term in the perturbative expansion of the interacting Green's functions. This approach is parameter free and completely *ab initio*,⁵ and in this paper will be addressed as *ab initio*-MBPT (*Ai*-MBPT) to

mark the difference with the conventional MBPT. However, the *Ai*-MBPT is a very cumbersome technique that, based on a perturbative concept, increases its level of complexity with the order of the expansion. As an example, this makes the extension of this approach beyond the linear response regime quite complex, although there have been recently some applications of the *Ai*-MBPT in nonlinear optics.^{8,9}

Another stringent restriction of the *Ai*-MBPT is that it can not be applied when nonequilibrium phenomena take place: for example, it can not be applied to study the light emission after an ultrafast laser pulse excitation. A generalization of MBPT to nonequilibrium situations has been proposed by Kadanoff and Baym.¹⁰ In their seminal works, the authors derived a set of equations for the real-time Green's functions, the Kadanoff-Baym equations (KBE's), that provide the basic tools of the nonequilibrium Green's function theory and allow essential advances in nonequilibrium statistical mechanics.¹⁰

Both the standard MBPT and nonequilibrium Green's function theory are based on the Green's function concept. This function describes the time propagation of a single-particle excitation under the action of an external perturbation. In the equilibrium MBPT, due to the time translation invariance, the relevant variable used to calculate the Green's functions is the frequency ω . Instead, out of equilibrium, in all non-steady-state situations, the time variables acquire a special role and much more attention is devoted to their propagation properties. The time propagation avoids the explosive dependence, beyond the linear response, of the MBPT on high-order Green's functions. Moreover, the KBE are nonperturbative in the external field, therefore, weak and strong fields can be treated on the same footing.

One of the first attempts to apply the KBE's for investigating optical properties of semiconductors was presented in the seminal paper of Schmitt-Rink and co-workers.¹¹ Later, the KBE's were applied to study quantum wells,¹² laser excited semiconductors,¹³ and luminescence.¹⁴ However, only recently it was possible to simulate the Kadanoff-Baym dynamics in real time.¹⁵⁻¹⁸

In this work, we combine a simplified version of the KBE's with DFT in such a way as to obtain a parameter-free theory that is able to reproduce and predict ultrafast and nonlinear phenomena (Sec. II). This approach, that we will address as time-dependent BSE, reduces to the standard BSE for weak perturbations (Sec. II C) but, at the same time, naturally describes optical excitations beyond the linear regime. After discussing some relevant aspects of the practical implementation of our approach (Sec. III), we exemplify how it works in practice by calculating the optical absorption spectra of *h*-BN and the time-dependent change in its electronic population due to the perturbation by means of an ultrafast and ultra-strong laser pulse (Sec. IV).

II. TIME-DEPENDENT BETHE-SALPETER EQUATION

We derive here an approach to solve the time evolution of an electronic system with Hamiltonian coupled with an external field,

$$\hat{H} = \hat{h} + \hat{H}_{mb} + \hat{U}, \quad (1)$$

where U represents the electron-light interactions (see Sec. III A for its specific form). As usually done in MBPT, \hat{H} is partitioned in an (effective) one-particle Hamiltonian \hat{h} and a part containing the many-particle effects \hat{H}_{mb} .

In our derivation, we take as a starting point the KBE's that we briefly introduce in Sec. II A (see, e.g., Ref. 19 for a systematic treatment). Then, in Sec. II B, we proceed in analogy with the equilibrium *Ai*-MBPT: first, we define \hat{h} as the Hamiltonian of the Kohn-Sham system, and second we introduce the same approximations for the self-energy operator. As result, we obtain an approach analogous to the successful *GW* + BSE one, for the non-equilibrium case. Indeed, in Sec. II C, we show that our approach, the time-dependent BSE, reduces to the *GW* + BSE in the linear regime.

A. Kadanoff-Baym equations

Within the KBE's, the time evolution of an electronic system coupled with an external field is described by the equation of motion for the nonequilibrium Green's functions^{10,19,20} $G(\mathbf{r}, t; \mathbf{r}', t')$. To keep the formulation as simple as possible, and being interested only in long-wavelength perturbations, we expand the generic G in the eigenstates $\{\varphi_{n,\mathbf{k}}\}$ of the \hat{h} Hamiltonian for a fixed momentum point \mathbf{k} :

$$[\mathbf{G}_{\mathbf{k}}(t_1, t_2)]_{n_1, n_2} \equiv G_{n_1, n_2, \mathbf{k}}(t_1, t_2) \\ = \int \varphi_{n_1, \mathbf{k}}^*(\mathbf{r}_1) G(\mathbf{r}_1, t_1; \mathbf{r}_2, t_2) \varphi_{n_2, \mathbf{k}}(\mathbf{r}_2) d^3 r_1 d^3 r_2. \quad (2)$$

As the external field does not break the spatial invariance of the system, \mathbf{k} is conserved.

Within a second-quantization formulation of the many-body problem, the equation of motion for the Green's function described by Eq. (2) is obtained from those for the creation and destruction operators. However, the resulting equations of motion for $\mathbf{G}_{\mathbf{k}}$ are not closed: they depend on the equations of the two-particle Green's function, which in turns depends on the three-particle Green's function and so on. In order to truncate this hierarchy of equations, one introduces the self-energy operator $\Sigma_{\mathbf{k}}(t_1, t_2)$, a nonlocal and frequency-dependent

one-particle operator that holds information of all higher-order Green's functions. A further complication arises with respect to the equilibrium case because of the lack of time-translation invariance in nonequilibrium phenomena, which implies that $\Sigma_{\mathbf{k}}(t_1, t_2)$ and $\mathbf{G}_{\mathbf{k}}(t_1, t_2)$ depend explicitly on both t_1, t_2 . Then, one can define an advanced $\Sigma_{\mathbf{k}}^a(\mathbf{G}_{\mathbf{k}}^a)$, a retarded $\Sigma_{\mathbf{k}}^r(\mathbf{G}_{\mathbf{k}}^r)$, a greater and a lesser $\Sigma_{\mathbf{k}}^>, \Sigma_{\mathbf{k}}^<(\mathbf{G}_{\mathbf{k}}^>, \mathbf{G}_{\mathbf{k}}^<)$ self-energy operators (Green's functions) depending on the ordering of t_1, t_2 on the time axis. Finally, the following equation for the $\mathbf{G}_{\mathbf{k}}^<$ is obtained (see, e.g., Chap. 2 of Ref. 19 for more details):

$$i\hbar \frac{\partial}{\partial t_1} G_{n_1, n_2, \mathbf{k}}^<(t_1, t_2) \\ = \delta(t_1 - t_2) \delta_{n_1, n_2} + h_{n_1, n_2, \mathbf{k}}(t_1) G_{n_1, n_2, \mathbf{k}}^<(t_1, t_2) \\ + \sum_{n_3} U_{n_1, n_3, \mathbf{k}}(t_1) G_{n_3, n_2, \mathbf{k}}^<(t_1, t_2) \\ + \sum_{n_3} \int dt_3 [\Sigma_{n_1, n_3, \mathbf{k}}^r(t_1, t_3) G_{n_3, n_2, \mathbf{k}}^<(t_3, t_2) \\ + \Sigma_{n_1, n_3, \mathbf{k}}^<(t_1, t_3) G_{n_3, n_2, \mathbf{k}}^a(t_3, t_2)]. \quad (3)$$

This equation, together with the adjoint one for $i\hbar \frac{\partial}{\partial t_2} G^<$, describes the evolution of the lesser Green's function $\mathbf{G}_{\mathbf{k}}^<$, which gives access to the electron distribution $[\mathbf{G}_{\mathbf{k}}^<(t, t)]$ and to the average of any one-particle operator such as, for example, the electron density [Eq. (10)], the polarization [Eq. (32)], and the current. However, in general $\Sigma^r, \Sigma^<$ and the $\mathbf{G}_{\mathbf{k}}^a$ depend on $\mathbf{G}_{\mathbf{k}}^>$, so that, in addition to Eq. (3), the corresponding equation for the $\mathbf{G}_{\mathbf{k}}^>$ has to be solved.

Then, in principle, to determine the nonequilibrium Green's function in presence of an external perturbation, one needs to solve the system of coupled equations for $\mathbf{G}_{\mathbf{k}}^>, \mathbf{G}_{\mathbf{k}}^<$, known as KBE's. Indeed, this system has been implemented within several approximations for the self-energy in model systems,^{15,16} in the homogeneous electron gas,¹⁷ and in atoms.¹⁸ The possibility of a direct propagation in time of the KBE's provided, in these systems, valuable insights on the real-time dynamics of the electronic excitations, as their lifetime and transient effects.¹⁵⁻¹⁸ Nevertheless, the enormous computational load connected to the large number of degrees of freedom *de facto* prevented the application of this method to crystalline solids, large molecules, and nanostructures. In the next section, we show a simplified approach, grounded on the DFT that, while capturing most of the physical effects we are interested in, makes calculation of "real-world" systems feasible.

B. Kohn-Sham Hamiltonian and an approximation for the self-energy

In analogy to *Ai*-MBPT for the equilibrium case, we choose as \hat{h} in Eq. (1) the Kohn-Sham Hamiltonian²¹

$$\hat{h} = -\frac{\hbar^2}{2m} \sum_i \nabla_i^2 + \hat{V}_{el} + \hat{V}^H[\bar{\rho}] + \hat{V}^{xc}[\bar{\rho}], \quad (4)$$

where \hat{V}_{el} is the electron-ion interaction, \hat{V}^H is the Hartree potential, and \hat{V}^{xc} the exchange-correlation potential. Within DFT, the Kohn-Sham Hamiltonian corresponds to the independent particle system that reproduces the ground-state

electronic density $\tilde{\rho}$ of the full interacting system ($\hat{h} + \hat{H}_{mb}$), that is,

$$\tilde{\rho} = \sum_{n\mathbf{k}} f_{n\mathbf{k}} |\varphi(\mathbf{r})|^2, \quad (5)$$

where $f_{n\mathbf{k}}$ is the Kohn-Sham Fermi distribution.

Equation (3) can be greatly simplified by choosing a static retarded approximation for the self-energy:

$$\Sigma^r(t_1, t_2) = [\Sigma^{\text{COHSEX}}(t_1) - \mathbf{V}_{xc}] \delta(t_1 - t_2), \quad (6a)$$

$$\Sigma^<(t_1, t_2) = 0, \quad (6b)$$

where the usual choice is Σ^{COHSEX} , the so-called Coulomb-hole plus screened-exchange self-energy (COHSEX). In Eq. (6a), we subtracted the correlation effects already accounted by Kohn-Sham Hamiltonian \hat{h} .²² The COHSEX is composed of two parts:

$$\Sigma^{\text{SEX}}(\mathbf{r}, \mathbf{r}', t) = iW(\mathbf{r}, \mathbf{r}'; G^<)G^<(\mathbf{r}, \mathbf{r}', t), \quad (7)$$

$$\Sigma^{\text{COH}}(\mathbf{r}, \mathbf{r}', t) = -W(\mathbf{r}, \mathbf{r}'; G^<)\frac{1}{2}\delta(\mathbf{r} - \mathbf{r}'), \quad (8)$$

where $W(\mathbf{r}, \mathbf{r}'; G^<)$ is the Coulomb interaction in the random-phase approximation (RPA), and $G^<(\mathbf{r}, \mathbf{r}', t)$ is the time-diagonal lesser Green's function $G^<(\mathbf{r}, \mathbf{r}', t) = G^<(\mathbf{r}, \mathbf{r}', t, t)$. These two terms are obtained as a static limit of the GW self-energy (see Chap. 4 of Ref. 19 and Refs. 22 and 23).

With the approximation in Eqs. (6a) and (6b), Eq. (3) does not depend anymore on $\mathbf{G}^>$. Moreover, since the COHSEX self-energy is local in time, and depends only on $G^<(\mathbf{r}, \mathbf{r}', t)$, Eq. (3) can be combined with the adjoint one for $\frac{\partial}{\partial t_2} G_{n_1 n_2 \mathbf{k}}^<(t_1, t_2)$ in such a way to have a closed equation in $t = (t_1 + t_2)/2$:

$$i\hbar \frac{\partial}{\partial t} G_{n_1, n_2, \mathbf{k}}^<(t) = [\mathbf{h}_{\mathbf{k}} + \mathbf{U}_{\mathbf{k}}(t) + \mathbf{V}_{\mathbf{k}}^H[\rho] - \mathbf{V}_{\mathbf{k}}^H[\tilde{\rho}] + (\Sigma_{\mathbf{k}}^{\text{COHSEX}}(t) - \mathbf{V}_{\mathbf{k}}^{\text{xc}}[\tilde{\rho}]), \mathbf{G}_{\mathbf{k}}^<(t)]_{n_1, n_2}, \quad (9)$$

where ρ is the density obtained from the $G^<$ as

$$\rho(\mathbf{r}, t) = \frac{i}{\hbar} \sum_{n_1 n_2 \mathbf{k}} \varphi_{n_1 \mathbf{k}}(\mathbf{r}) \varphi_{n_2 \mathbf{k}}^*(\mathbf{r}) G_{n_2 n_1 \mathbf{k}}^<(t). \quad (10)$$

After reducing to a single time, Eq. (9) is equivalent to a density matrix approach with a potential local in time. However, despite that the full real-time COHSEX dynamics [Eq. (9)] is an appealing option considerably simplifying the dynamics with respect to the KBE's, it neglects the dynamical dependence of the self-energy operator. This, in practice, induces a consistent renormalization of the quasiparticle charge⁷ in addition to an opposite enhancement of the optical properties.²⁴ In the COHSEX approximation, both effects are neglected. At the level of response properties for most of the extended systems, dynamical effects are either negligible or very small (while recently it has been shown their importance for finite systems, see Refs. 25 and 26) and, for practical purposes, it has been shown that they partially cancel with the quasiparticle renormalization factors.²⁴

Therefore, we modify Eq. (9) in order to include only the effect of the dynamical self-energy on the renormalization of the quasiparticle energies, which is the most important effect. Also in this case, our idea is to proceed in strict analogy with *Ai*-MBPT and to derive a real-time equation that reproduces

the fruitful combination of the G_0W_0 approximation (for the one-particle Green's function) and of the BSE with a static self-energy (for the two-particle Green's function). Indeed the $G_0W_0 + \text{BSE}$ is the state-of-the-art approach to study optical properties within the *Ai*-MBPT.⁵ To this purpose, Eq. (9) is modified as

$$i\hbar \frac{\partial}{\partial t} G_{n_1 n_2 \mathbf{k}}^<(t) = [\mathbf{h}_{\mathbf{k}} + \Delta \mathbf{h}_{\mathbf{k}} + \mathbf{U}_{\mathbf{k}} + \mathbf{V}_{\mathbf{k}}^H[\rho] - \mathbf{V}_{\mathbf{k}}^H[\tilde{\rho}] + \Sigma_{\mathbf{k}}^{\text{COHSEX}}[G^<] - \Sigma_{\mathbf{k}}^{\text{COHSEX}}[\tilde{G}^<], \mathbf{G}_{\mathbf{k}}^<(t)]_{n_1 n_2}, \quad (11)$$

where $\tilde{G}^<$ is the solution for the unperturbed system ($U = 0$) (Ref. 27):

$$\tilde{G}_{n\mathbf{k}}^< = i\hbar f_{n\mathbf{k}} \delta_{nn'}. \quad (12)$$

To obtain Eq. (11), we subtracted from Eq. (9) the static quasiparticle correction of the system at equilibrium ($U = 0$), $\Sigma_{\mathbf{k}}^{\text{COHSEX}}[\tilde{G}^<] - V^{\text{xc}}[\tilde{\rho}]$, and added the scissor operator⁵ $\Delta \mathbf{h}$ that applies the G_0W_0 correction to the Kohn-Sham eigenvalues $e_{n\mathbf{k}}^{\text{KS}}$:

$$[\Delta \mathbf{h}_{\mathbf{k}}]_{n_1, n_2} = (e_{n_1 \mathbf{k}}^{G_0W_0} - e_{n_1 \mathbf{k}}^{\text{KS}}) \delta_{n_1, n_2}. \quad (13)$$

Equation (11) is the key result of this work. In practice, it assumed that quasiparticle dynamical effects are frozen to their value at equilibrium. On the other hand, the $\Sigma_{\mathbf{k}}^{\text{COHSEX}}[G^<] - \Sigma_{\mathbf{k}}^{\text{COHSEX}}[\tilde{G}^<]$ operator appearing in Eq. (11) includes correlation effects induced by the external field, which are responsible, for example, for the band-gap shrinking.²⁸

In the following section, we show how in the linear response limit, this approximation corresponds to the $G_0W_0 + \text{BSE}$, which within *Ai*MBPT is very successful for a wide range of materials characterized by weak correlations (see, e.g., Refs. 5 and 6).

C. Linear response limit

When an external perturbation $U(t)$ is switched on in Eq. (11), it induces a variation of the Green's function, $\Delta \mathbf{G}_{\mathbf{k}}^<(t) = \mathbf{G}_{\mathbf{k}}^<(t) - \tilde{\mathbf{G}}_{\mathbf{k}}^<$. In turn, this variation induces a change in the self-energy and in the Hartree potential. In the case of a strong applied laser field, these changes depend on all possible orders in the external field. However, for weak fields, the linear term is dominant. In this regime, it is possible to show analytically that Eq. (11) reduces to the $G_0W_0 + \text{BSE}$ approach.^{3,6} Proceeding similarly to Ref. 25, we consider the retarded density-density correlation function

$$\chi^r(\mathbf{r}, t; \mathbf{r}', t') = -i[\langle \rho(\mathbf{r}, t) \rho(\mathbf{r}', t') \rangle - \langle \rho(\mathbf{r}, t) \rangle \langle \rho(\mathbf{r}', t') \rangle] \theta(t - t'). \quad (14)$$

χ^r describes the linear response of the system (initially at equilibrium) to a weak perturbation, represented in Eq. (1) by U :

$$\chi^r(\mathbf{r}, t; \mathbf{r}', t') = \left. \frac{\langle \delta \rho(\mathbf{r}t) \rangle}{\delta U(\mathbf{r}'t')} \right|_{U=0}. \quad (15)$$

We start by expanding χ^r in terms of the Kohn-Sham orbitals

$$\chi^r(\mathbf{r}, t; \mathbf{r}', t'; \mathbf{q}) = \sum_{\substack{i,j,\mathbf{k} \\ l,m,\mathbf{k}' \\ l,m,\mathbf{k}}} \chi_{i,j,\mathbf{k}}^r(t, t'; \mathbf{q}) \\ \times \varphi_{i,\mathbf{k}}(\mathbf{r}) \varphi_{j,\mathbf{k}+\mathbf{q}}^*(\mathbf{r}) \varphi_{l,\mathbf{k}'}^*(\mathbf{r}') \varphi_{m,\mathbf{k}'+\mathbf{q}}(\mathbf{r}'), \quad (16)$$

where \mathbf{q} is the momentum, and we define the matrix elements of χ^r as,

$$\chi_{ij,\mathbf{k}}^r(t, t'; \mathbf{q}) = \iint d^3r d^3r' \chi^r(\mathbf{r}, t; \mathbf{r}', t'; \mathbf{q}) \times \varphi_{i,\mathbf{k}}^*(\mathbf{r}) \varphi_{m,\mathbf{k}'}^* \\ + \mathbf{q}(\mathbf{r}') \varphi_{j,\mathbf{k}+\mathbf{q}}(\mathbf{r}) \varphi_{l,\mathbf{k}'}(\mathbf{r}'). \quad (17)$$

Since we are interested only in the optical response, in what follows we restrict ourselves to the case $\mathbf{q} = 0$ and drop the \mathbf{q} dependence of χ^r (for the extension to finite momentum transfer, see Ref. 17). By inserting the expansion for χ [Eq. (16)], ρ [Eq. (10)], and U ($U_{mn,\mathbf{k}} \equiv \langle m\mathbf{k} | U | n\mathbf{k} \rangle$) in Eq. (15), we obtain the following relation linking the matrix elements of χ^r to the matrix elements of $G^<$:

$$\chi_{ij,\mathbf{k}}^r(t, t') = \left. \frac{\delta \langle i G_{ji,\mathbf{k}}^<(t) \rangle}{\delta U_{lm,\mathbf{p}}(t')} \right|_{U=0}. \quad (18)$$

Then, we can obtain the equation of motion for the matrix elements of χ^r by taking the functional derivative of Eq. (11) with respect to $U_{l,m,\mathbf{k}}(t)$:

$$-i\hbar \frac{\partial}{\partial t} \chi_{ij,\mathbf{k}}^r(t, t') \\ = \frac{\delta}{\delta U_{lm,\mathbf{p}}(t')} (\mathbf{h}_{\mathbf{k}} + \Delta \mathbf{h}_{\mathbf{k}} + \mathbf{U}_{\mathbf{k}}(t) + \mathbf{V}_{\mathbf{k}}^H[\rho(t)] \\ - \mathbf{V}_{\mathbf{k}}^H[\bar{\rho}] + \Sigma_{\mathbf{k}}[G^<(t)] - \Sigma_{\mathbf{k}}[\tilde{G}^<], \mathbf{G}_{\mathbf{k}}^<(t))_{ji}. \quad (19)$$

Making use of the definitions in Eqs. (13) and (12), together with Eq. (18), it can be verified that the functional derivative of the one-electron Hamiltonian and of the external field give the contribution

$$\frac{\delta}{\delta U_{l,m,\mathbf{p}}(t')} [\mathbf{h}_{\mathbf{k}} + \Delta \mathbf{h}_{\mathbf{k}} + \mathbf{U}_{\mathbf{k}}, \mathbf{G}_{\mathbf{k}}^<(t)]_{ji} \Big|_{U=0} \\ = (e_{j\mathbf{k}}^{G_0 W_0} - e_{i\mathbf{k}}^{G_0 W_0}) \chi_{ji,\mathbf{k}}^r(t - t') \\ + i(f_{i\mathbf{k}} - f_{j\mathbf{k}}) \delta_{jl} \delta_{im} \delta_{\mathbf{k}\mathbf{p}} \delta(t - t'). \quad (20)$$

Note that χ^r is invariant with respect to time translations (χ^r depends only on $t - t'$) since the functional derivative in Eq. (20), as in the rest of the section, is evaluated at equilibrium ($U = 0$), and the unperturbed Hamiltonian does not depend on time. The term in Eq. (19) containing the Hartree potential, which is not directly depending on the external perturbation, is expanded with respect to $U_{l,m,\mathbf{k}}(t)$ by using the functional derivative chain rule and the definition of χ^r given by Eq. (18) as

$$\delta V_{ij,\mathbf{k}}^H[\rho(t)] = \sum_{\substack{n,n',\mathbf{p} \\ l,m,\mathbf{k}'}} \iint dt' dt'' \frac{\delta V_{ij,\mathbf{k}}^H[\rho(t)]}{\delta G_{n',\mathbf{p}}^<(t')} \\ \times \chi_{n,n',\mathbf{p}}^r(t', t'') \delta U_{lm,\mathbf{k}'}(t''). \quad (21)$$

A similar equation can be obtained for $\Sigma_{ij,\mathbf{k}}^{\text{COHSEX}}[G^<(t)]$. Equation (21) for the Hartree potential and its analogy for the self-energy can be explicitated by using

$$V_{mn,\mathbf{k}}^H(t) = -2i \sum_{ij} G_{ji,\mathbf{k}}^<(t) v_{mn,\mathbf{k}}^{q=0}, \quad (22)$$

$$\Sigma_{mn,\mathbf{k}}^{\text{COHSEX}}(t) = i \sum_{ij,\mathbf{q}} G_{ji,(k-\mathbf{q})}^<(t) W_{m\mathbf{k},i(k-\mathbf{q})}^{nk,j(k-\mathbf{q})}, \quad (23)$$

where the matrix elements of $v^{q=0}$ and W are labeled accordingly to Eq. (17). In Eq. (22), $v^{q=0}$ is the long-range part of the bare Coulomb potential, responsible for the local field effects in the BSE. Then, by inserting Eq. (22) in (21), the functional derivative for the Hartree term is

$$\frac{\delta}{\delta U_{lm,\mathbf{p}}(t')} [\mathbf{V}_{\mathbf{k}}^H[\rho(t)] - \mathbf{V}_{\mathbf{k}}^H[\bar{\rho}], \mathbf{G}_{\mathbf{k}}^<(t)]_{ji} \Big|_{U=0} \\ = (2i^2)(f_{i\mathbf{k}} - f_{j\mathbf{k}}) \sum_{st} v_{ji,\mathbf{k}}^{q=0} \chi_{st,\mathbf{k}}^r(t - t'). \quad (24)$$

Similarly, an analogous equation is obtained for the self-energy (see also the Appendix)

$$\frac{\delta}{\delta U_{lm,\mathbf{p}}(t')} [\Sigma_{\mathbf{k}}[G^<(t)] - \Sigma_{\mathbf{k}}[G^<(t)], \mathbf{G}_{\mathbf{k}}^<(t)]_{ji} \Big|_{U=0} \\ = (-i^2)(f_{i\mathbf{k}} - f_{j\mathbf{k}}) \sum_{st,\mathbf{q}} W_{j\mathbf{k},s(\mathbf{k}-\mathbf{q})}^{ik,t(\mathbf{k}-\mathbf{q})} \chi_{st,\mathbf{k}}^r(t - t'), \quad (25)$$

where we neglected the part containing the functional derivative of the screened interaction with respect to the external perturbation. This is a basic assumption of the standard BSE that is introduced in order to neglect high-order vertex corrections.³

Finally, we insert Eqs. (20), (24), and (25) in Eq. (19), and by Fourier transforming with respect to $(t - t')$, we obtain

$$[\hbar\omega - (\epsilon_{j\mathbf{k}}^{G_0 W_0} - \epsilon_{i\mathbf{k}}^{G_0 W_0})] \chi_{ij,\mathbf{k}}^r(\omega) \\ = i(f_{i\mathbf{k}} - f_{j\mathbf{k}}) \left[\delta_{jl} \delta_{im} \delta_{\mathbf{k}\mathbf{p}} \right. \\ \left. + i \sum_{st,\mathbf{q}} \left\{ W_{j\mathbf{k},s(\mathbf{k}-\mathbf{q})}^{ik,t(\mathbf{k}-\mathbf{q})} - 2v_{ji,\mathbf{k}}^{q=0} \right\} \chi_{st,\mathbf{k}-\mathbf{q}}^r(\omega) \right], \quad (26)$$

formally equivalent to the standard BSE.

III. OPTICAL PROPERTIES FROM A TIME-DEPENDENT APPROACH

A. Practical solution of the time-dependent BSE

To solve Eq. (11) for a given electronic system [Eq. (1)], we start from \hat{h} , with its eigenvalues and eigenstates determined from a previous DFT calculation, and from the corrections $\Delta \mathbf{h}_{\mathbf{k}}$, determined, e.g., from a previous $G_0 W_0$ calculation. Then, we switch on the external perturbation U and integrate the equations of motion using the same scheme as in Ref. 15 for the diagonal part of the $G^<$, which is equivalent to a second-order Runge-Kutta integration scheme. Specifically, in Eq. (1), we choose to treat the interaction with the external

electric field \mathbf{E} within the direct coupling, or length gauge,

$$\hat{U} = -e\hat{\mathbf{r}} \cdot \mathbf{E}(t). \quad (27)$$

Other choices are possible and indeed in the literature, the electron-light interaction is often described within the minimal coupling, or velocity gauge ($\hat{\mathbf{p}} \cdot \mathbf{A}$), with \mathbf{A} the vector potential. As it has been pointed out in Ref. 29, the length and velocity gauges lead to the same results only if a gauge transformation is correctly applied. However, in this respect, the velocity gauge presents two main drawbacks. First, the wave functions and the boundary conditions have to be transformed by a time-dependent gauge factor $T(\mathbf{r},t) = \exp\{i\mathbf{A}(t) \cdot \hat{\mathbf{r}}\}$ and, accordingly, in the Green's function formalism also the self-energy and the dephasing term have to be transformed. Second, within perturbation theory, the velocity gauge induces divergent terms in the response function that in principle cancel each other, but that in practice lead to artificial divergences in the optical response^{1,30} due to numerical precision and incomplete basis sets.

The interaction Hamiltonian U is evaluated in terms of unperturbed Kohn-Sham eigenfunctions as

$$\langle m\mathbf{k}|U|n\mathbf{k}\rangle = -\mathbf{E}(t)\langle m\mathbf{k}|\mathbf{r}|n\mathbf{k}\rangle = -\mathbf{E}(t)\mathbf{r}_{mn,\mathbf{k}}, \quad (28)$$

where the dipole matrix elements $\mathbf{r}_{mn,\mathbf{k}}$, for $m \neq n$ are calculated by using the commutation relation $i[H,\mathbf{r}] = \mathbf{p} + i[V_{nl},\mathbf{r}]$, where V_{nl} is the nonlocal part of the Hamiltonian operator.³¹

Since we are interested in calculating the dielectric properties at zero momentum, we choose to work with a homogeneous electric field $\mathbf{E}(t)$, with no space dependence except its direction,¹ generated by a vector potential $\mathbf{A}(t)$ constant in space,

$$\mathbf{E}(t) = -\frac{1}{c} \frac{d\mathbf{A}(t)}{dt}. \quad (29)$$

Also in this case, other choices consistent with the periodic boundary conditions would be possible as, for example, an external potential with the cell periodicity,³² or an electric field with a finite momentum¹⁷ \mathbf{q} such that $\mathbf{q} = \mathbf{k} - \mathbf{k}'$.

Instead, the particular form of $\mathbf{E}(t)$ as a function of time is not specified *a priori*, but given as an input parameter of the simulation. Indeed, the possibility of providing the form of the external field as an input is one of the key strengths of the real-time approach, potentially allowing us to use the same implementation to simulate a broad range of phenomena and of experimental techniques. For example, as described in Sec. IV, in order to calculate the linear optical susceptibility spectrum $\chi(\omega)$, we will use a delta function $\mathbf{E}(t) = \mathbf{E}_0\delta(t - t_0)$ [obtained from Eq. (29) with $\mathbf{A}(t) = A_0\Theta(t - t_0)$, where t_0 is the time at which the external field is switched on] and $\Theta(t)$ is the Heaviside step function. This electric field probes the system at all frequencies with the same intensity. Also, in the other example described in Sec. IV, we can use a quasimonochromatic source $\mathbf{E}(t) = \mathbf{E}_0 \sin \omega_0 t \exp[-\delta^2(t - t_0)^2/2]$ to selectively excite the system at a given frequency ω_0 . Furthermore, two or more electric fields can be used to simulate, e.g., pump-probe, sum-of-frequency, or wave-mixing experiments.

The macroscopic quantity that is calculated at the end of the real-time simulation is the induced polarization $\mathbf{P}(t)$, related to the electric displacement $\mathbf{D}(\mathbf{r},t)$ and the electric field $\mathbf{E}(\mathbf{r},t)$

by the so-called material equation

$$\mathbf{D}(\mathbf{r},t) = \epsilon_0\mathbf{E}(\mathbf{r},t) + \mathbf{P}(\mathbf{r},t), \quad (30)$$

which stems directly from the Maxwell equations. $\mathbf{P}(t)$ is obtained from $G^<$ [Eq. (11)] by

$$\mathbf{P}(t) = -\frac{1}{V} \sum_{n,m,\mathbf{k}} r_{mn,\mathbf{k}} G_{nm,\mathbf{k}}^<(t), \quad (31)$$

and from this quantity we can obtain the optical properties of the system under study.

For instance, within linear response, the electric displacement $\mathbf{D}(\mathbf{r},t)$ is directly proportional, in frequency space, to the electric field as $\mathbf{D}(\omega) = \hat{\epsilon}(\omega)\epsilon_0\mathbf{E}(\omega)$. Therefore, the polarization can be expressed as

$$\mathbf{P}(\omega) = \epsilon_0[\hat{\epsilon}(\omega) - \hat{I}]\mathbf{E}(\omega) \quad (32)$$

and, accordingly, the optical susceptibility that describes the linear response of the system to a perturbation is $\hat{\chi}(\omega) = \hat{\epsilon}(\omega) - \hat{I}$. Then, the optical susceptibility $\hat{\chi}(\omega)$ can be calculated by Fourier transforming the macroscopic polarization $\mathbf{P}(\omega)$ [or alternatively the current density $\mathbf{j}(\omega)$], by means of Eq. (32) as

$$\hat{\chi}(\omega) = \frac{\mathbf{P}(\omega)}{\epsilon_0\mathbf{E}(\omega)}. \quad (33)$$

Note that by choosing a deltalike $\mathbf{E}(t)$, the Fourier transform of $\mathbf{P}(t)$ provides directly the full spectrum of the optical susceptibility $\hat{\chi}(\omega)$.³³ Beyond the linear regime, higher-order response functions $\hat{\chi}^{(2)}, \hat{\chi}^{(3)}, \dots$ can be obtained (to calculate, e.g., the second- or third-harmonic generation) by using a (quasi)monochromatic field as, e.g., in Ref. 4; nonperturbative phenomena, such as high-harmonic generation, can be analyzed instead from the power spectrum ($|P(\omega)|^2$).

To summarize, the schematic flow of a time-dependent BSE simulation is shown in Fig. 1, as has been implemented in the YAMBO code.³⁴

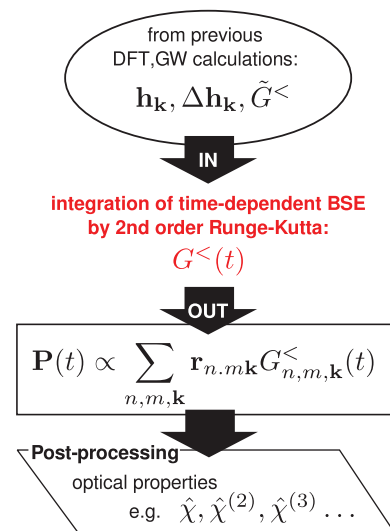


FIG. 1. (Color online) Schematic flow of a time-dependent BSE simulation. See Sec. III A for details.

B. Dissipative effects

In an excited electronic system, dissipative effects are present due to inelastic electron scattering and (quasi)elastic scattering processes with other degrees of freedom, such as defects or phonons. Both effects contribute to the relaxation and decay of excited electronic population as well as of the decay of phase coherence, that is, to a finite dephasing rate. Our approach, Eq. (11), does not account for dissipative effects: on the one hand, the COHSEX self-energy is real, so that the excitations lifetimes are infinite; on the other hand, the electronic systems are perfectly isolated [Eq. (1)], so that there is no dephasing due to interaction with other degrees of freedom.

In practical calculations, then we introduce a phenomenological damping to simulate dissipative effects. We implemented two different approaches: an *a posteriori* treatment, where at the end of the simulation (in the post-processing block of Fig. 1), the polarization (and the electric field) are multiplied by a decaying exponential function $e^{-t/\tau}$, where τ is an empirical parameter. This parameter, which is compatible with the simulation length, effectively simulates the dephasing and introduces a Lorentzian broadening in the resulting absorption spectrum. This is in the same spirit of the Lorentzian broadening introduced in the linear response treatment to simulate the experimental optical spectra, and has the advantage of producing spectra with different broadening from the same

real-time simulation. Nevertheless, this approach is limited to the linear response case.

In order to treat dissipative effects beyond the linear regime, an imaginary term is added to the self-energy in the form of an additional term $\Gamma_{\mathbf{k}}(\mathbf{G}_{\mathbf{k}}^<(t) - \tilde{\mathbf{G}}_{\mathbf{k}}^<)$ appearing on the right-hand side of Eq. (11), with

$$i[\Gamma_{\mathbf{k}}]_{n_1, n_2} = \Gamma_{n_1 \mathbf{k}}^{ph} + \Gamma_{n_2 \mathbf{k}}^{ph} + \Gamma_{n_1 \mathbf{k}}^{\text{pop}} \delta_{n_1, n_2}, \quad (34)$$

where $\Gamma_{n_1 \mathbf{k}}^{\text{pop}}$ and $\Gamma_{n_1 \mathbf{k}}^{ph}$ are, respectively, the lifetime of the perturbed electronic population and the dephasing rate, and are given as input parameters of the simulation.

IV. EXAMPLES

To illustrate and validate the time-dependent BSE approach and our numerical implementation, we present two examples on *h*-BN. This is a wide gap insulator, the optical properties of which are strongly renormalized by excitonic effects and for which all the parameters necessary in DFT, G_0W_0 , and response calculations³⁵ are known from previous studies.³⁶

In these examples, we used Eq. (11), with and without including the self-energy term. We refer to the former approximation as TD-BSE, and to the latter as TD-HARTREE. Within equilibrium MBPT, these two approximations would correspond to the BSE and RPA, and in fact they reduce to BSE and RPA within the linear response limit (Sec. II C).

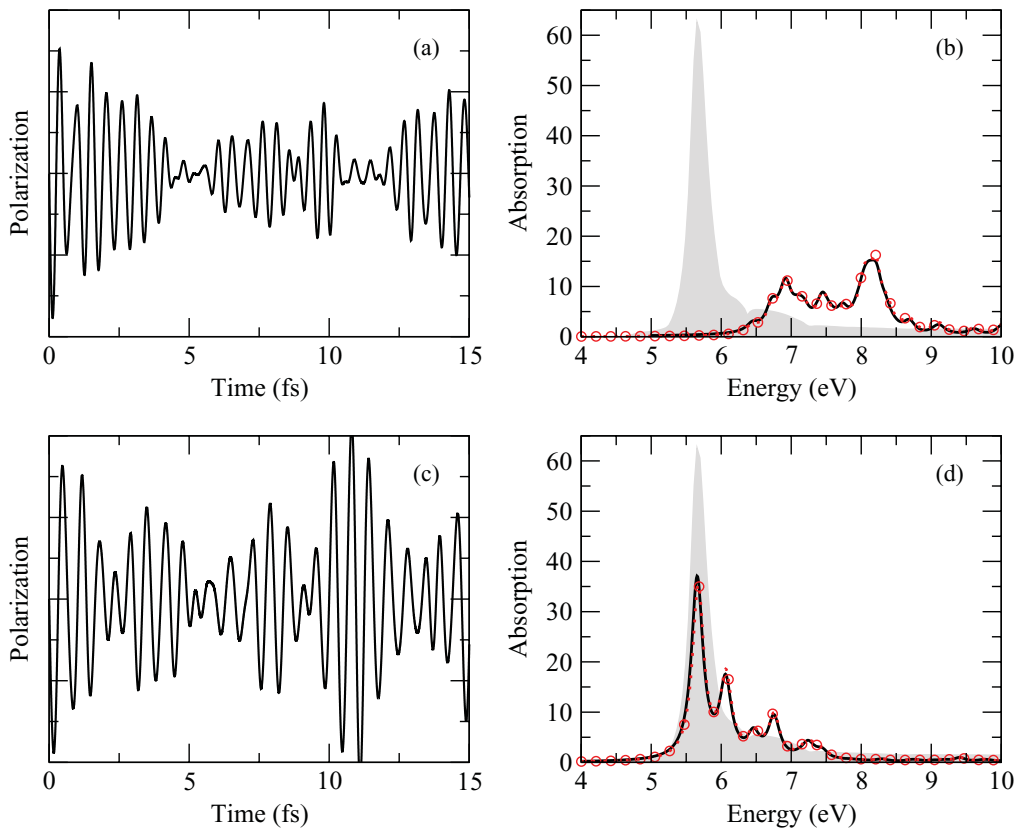


FIG. 2. (Color online) *h*-BN: Comparison between the real-time approach and the standard RPA and BSE approaches based on the equilibrium MBPT. (a), (c): Polarization $\mathbf{P}(t)$ generated by an electric field $\mathbf{E}(t) = \mathbf{E}_0 \delta(t)$ within the TD-HARTREE [(a)] and TD-BSE [(c)] approximations. (b), (d): The corresponding absorption spectra (red circles) are compared with the RPA [(b)] and with the BSE [(d)] results (black line). The experimental absorption spectrum (gray shadow) is also shown as reference.

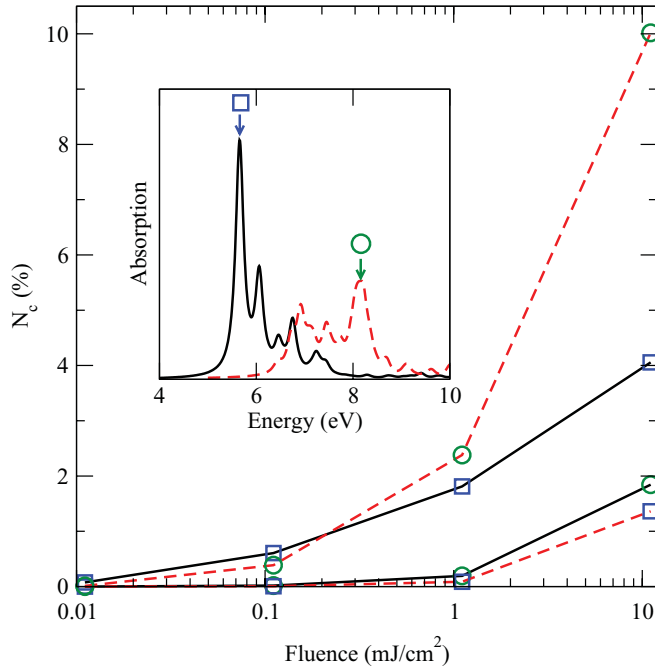


FIG. 3. (Color online) *h*-BN: Percentage of valence electrons pumped to the conduction bands (N_c) by a quasimonochromatic pulse as a function of the fluence. The pulse is centered either at 5.65 eV (blue boxes) or 8.1 eV (green circles) calculated within the TD-BSE (black line) and the td-HARTREE (red dashed line) approximations. In either case, each point corresponds to a separate simulation and the lines are drawn to help guide the eye. The inset shows the absorption spectra within the TD-BSE (black line) and TD-HARTREE (red dashed line) with the arrows pointing at the pump frequencies.

In the first example (Fig. 2), we simulated *h*-BN interacting with a weak deltalike laser field.³⁷ As explained in Sec. III A, a deltalike laser field probes all frequencies of the system and the Fourier transform of the macroscopic polarizability provides directly the susceptibility [Eq. (33)] and thus the dielectric constant [Eq. (32)]. Since we use a weak field, we expect negligible nonlinear effects. Then, accordingly with Sec. II C, the results from TD-BSE and TD-HARTREE can be directly compared with the BSE and RPA within the standard *Ai*-MBPT approach. Indeed, in Figs. 2(b) and 2(d), the imaginary part of the dielectric constant (optical absorption) obtained by Fourier transform of the polarization in Figs. 2(a) and 2(c) is indistinguishable from that obtained within equilibrium *Ai*-MBPT, validating our numerical implementation.

In the second example (Figs. 3 and 4), we exploit the potentiality of the TD-BSE approach by going beyond the linear regime and using a strong quasimonochromatic laser field (see Sec. III A). This field excites the system selectively at one given frequency, moreover, it is strong enough to induce changes in the electronic population of the system. To track these changes, during the dynamics we followed the evolution of $N_c(\%)$, that is, the percentage of valence electrons that are pumped by the electric field in the conduction bands (in our simulation, we have 16 valence electrons in the *h*-BN unit cell since core electrons are accounted for using pseudopotentials). The total number of valence electrons in the system is given by the trace of $G^<$, while $N_c(t) = -i \sum_{ck} G_{cck}^<(t)$, where c labels the empty states in the unperturbed system.

We performed the simulations³⁷ for fields intensities in the range of 10^6 – 10^9 kW/cm² and for two values of the field

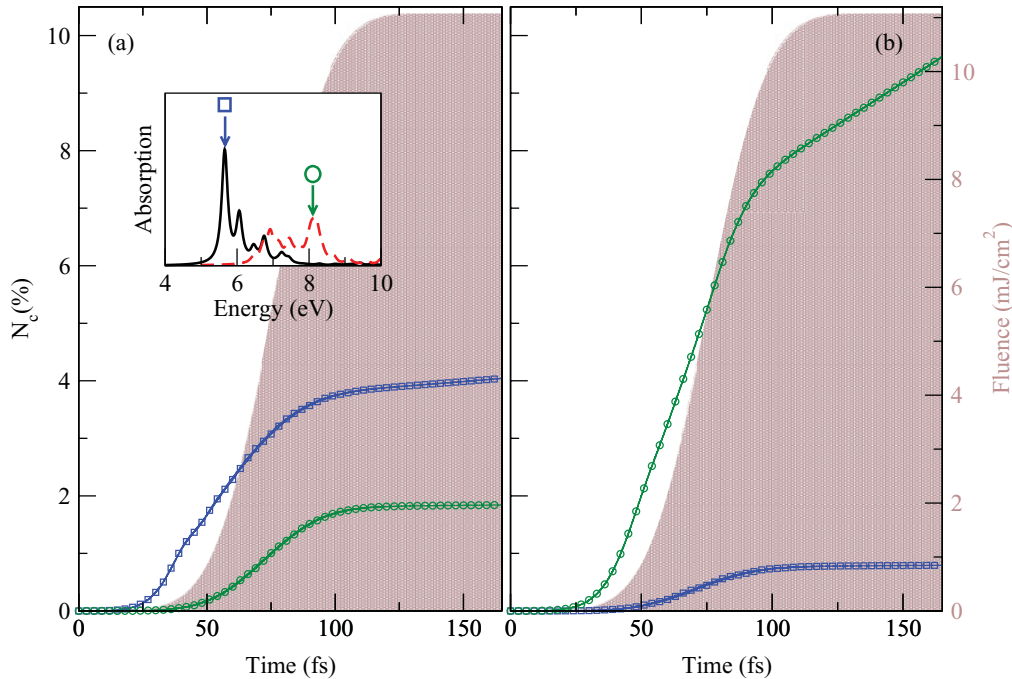


FIG. 4. (Color online) *h*-BN: Percentage as function of time of valence electrons pumped to the conduction bands (N_c) by a quasimonochromatic pulse with field strength of 1.94×10^9 V/m centered either at 5.65 eV (blue boxes) or 8.1 eV (green circles) and calculated either within the TD-BSE [(a)] or the TD-HARTREE [(b)] approximations. The brown shadow represents the fluence as a function of time. The inset shows the absorption spectra within the TD-BSE (black line) and TD-HARTREE (red dashed line) with the arrows pointing at the pump frequencies.

frequency, 5.65 and 8.1 eV, that, depending on the level of the theory, are either at resonance or off resonance with the system characteristic frequencies. More precisely, within TD-BSE, 5.65 eV corresponds to the strong excitonic feature in the absorption spectrum, while at 8.1 eV, the absorption is negligible; conversely, within RPA at 5.65 eV, the absorption is negligible, while 8.1 eV corresponds to the strongest feature in the spectrum (see inset of Figs. 3 and 4). The results of the various simulations are summarized in Fig. 3, which shows $N_c(\%)$ as a function of the fluence, i.e., the pulse energy per unit area. For a comparison, the ablation threshold of *h*-BN has been determined as 78 mJ/cm² in the femtosecond laser operational mode.³⁸

Finally, Figs. 4(a) and 4(b) show the evolution of $N_c(\%)$ during the simulation for a field strength of 1.94×10^9 V/m: one can clearly observe the enhancement in the electronic-population change due to resonance effects. The very different picture that is obtained within the two different approximations emphasizes the importance of accounting for excitonic effects (also) in the strong-field regime.

V. SUMMARY

We presented an approach to the *ab initio* calculation of optical properties in bulk materials and nanostructures that uses a time-dependent extension of the BSE. The proposed approach combines the flexibility of a real-time approach with the strength of MBPT in capturing electron correlation. It allows us to perform computationally feasible simulations beyond the linear regime of, e.g., second- and third-harmonic generation, four-wave mixing, Fourier spectroscopy, or pump-probe experiments. Furthermore, being the approach based on the nonequilibrium Green's function theory, it is possible to include effects such as lifetimes, electron-electron scattering²⁵ and electron-phonon coupling³⁹ in a systematic way. Finally, we have applied the TD-BSE to the case of *h*-BN. First, we have calculated the optical absorption and compared it with the results from equilibrium *Ai*-MBPT, validating our approach and numerical implementation. Then, we have shown the potentialities of the TD-BSE approach beyond the linear regime by calculating the change in the electronic population due to the interaction with a strong quasimonochromatic laser field.

ACKNOWLEDGMENTS

C.A. acknowledges useful discussions on this work with I. Tokatly and L. Stella. The authors acknowledge funding by the European Community through e-I3 ETSF project (Contract No. 211956). A.M. acknowledges support from the HPC-Europa2 transnational programme (application No. 819). M.G. acknowledges support from the Fundação para a Ciência e a Tecnologia (FCT) through the Ciência 2008 programme. This work was performed using HPC resources

of the GENCI-IDRIS Project No. 100063, of the CIMENT platform in Grenoble, of the CASPUR HPC in Rome, and of the Laboratory of Advanced Computation of the University of Coimbra.

APPENDIX: AN EFFICIENT METHOD TO UPDATE THE COHSEX SELF-ENERGY DURING THE TIME EVOLUTION

In this appendix, we show how we store and update the Σ^{COHSEX} self-energy in an efficient manner. First of all, we neglect the variation of the screened interaction $W(\mathbf{r}, \mathbf{r}'; G^<(t))$ with respect to the $G^<(\mathbf{r}, \mathbf{r}', t)$ by setting to zero the functional derivative $\partial W / \partial G$ (see Sec. II C). Within this approximation, the Σ^{COH} does not contribute to the time evolution, therefore, only Σ^{SEX} needs to be updated:

$$\Sigma^{\text{SEX}}(\mathbf{r}, \mathbf{r}', t) = i W(\mathbf{r}, \mathbf{r}') \sum_{n, n', \mathbf{k}} \varphi_{n, \mathbf{k}}(\mathbf{r}) \varphi_{n', \mathbf{k}}^*(\mathbf{r}') G_{n, n', \mathbf{k}}^<(t). \quad (\text{A1})$$

The KBE involves the matrix elements $\langle m, \mathbf{k} | \Sigma^{\text{SEX}} | m', \mathbf{k} \rangle$:

$$\Sigma_{m, m', \mathbf{k}}^{\text{SEX}}(t) = \sum_{\substack{\mathbf{G}, \mathbf{G}', \mathbf{q} \\ n, n'}} \rho_{m, n}(\mathbf{G}') \rho_{m', n'}^*(\mathbf{G}) W_{\mathbf{G}, \mathbf{G}'(\mathbf{q})} G_{n, n', \mathbf{k}-\mathbf{q}}^<(t), \quad (\text{A2})$$

where

$$\rho_{m, n}(\mathbf{G}) = \int \varphi_{m, \mathbf{k}}^*(\mathbf{r}) \varphi_{n, \mathbf{k}-\mathbf{q}}(\mathbf{r}) e^{i(\mathbf{G}+\mathbf{q})\mathbf{r}}. \quad (\text{A3})$$

In order to rapidly update Σ^{SEX} after a variation of $G^<(\mathbf{r}, \mathbf{r}', t)$, we store the matrix elements

$$M_{m, m', n, n'} = \sum_{\mathbf{q}, \mathbf{k}} \rho_{m, n}(\mathbf{k}, \mathbf{q}, \mathbf{G}') \rho_{m', n'}^*(\mathbf{k}, \mathbf{q}, \mathbf{G}) W_{\mathbf{G}, \mathbf{G}'(\mathbf{q})}, \quad (\text{A4})$$

in such a way that $\Sigma_{m, m'}^{\text{SEX}}$ can be rewritten as

$$\Sigma_{m, m', \mathbf{k}}^{\text{SEX}}(t) = \sum_{\substack{n, n' \\ \mathbf{q}}} M_{m, m', n, n'} \cdot G_{n, n', \mathbf{k}-\mathbf{q}}^<(t). \quad (\text{A5})$$

The M matrix can be very large, but its size can be reduced by noticing that (i) the matrix M is Hermitian with respect to the (m, m') indexes; (ii) the number of \mathbf{k} and \mathbf{q} points is reduced by applying the operation symmetries that are left unaltered by the applied external field; (iii) for converging optical properties, only the bands close to the gap are needed (see Sec. IV). As an additional numerical simplification, we neglected all terms such that $M_{m, m', n, n'} / \max_{\mathbf{q}, \mathbf{k}} \{M_{m, m', n, n'}\} <$

M_c , where M_c is a cutoff that, if chosen to be $M_c \simeq 5 \times 10^{-3}$, does not appreciably affect the final results. In principle, by using an auxiliary localized basis set,⁴⁰ one can obtain a further reduction of the matrix dimensions, but in the present work we did not explore this strategy.

¹G. F. Bertsch, J.-I. Iwata, A. Rubio, and K. Yabana, *Phys. Rev. B* **62**, 7998 (2000).

²A. Castro, H. Appel, M. Oliveira, C. A. Rozzi, X. Andrade, F. Lorenzen, M. A. L. Marques, E. K. U. Gross,

and A. Rubio, *Phys. Status Solidi B* **243**, 2465 (2006); J. Sun, J. Song, Y. Zhao, and W.-Z. Liang, *J. Chem. Phys.* **127**, 234107 (2007).

³Q. G. Strinati, *Riv. Nuovo Cimento* **11**, 1 (1998).

- ⁴Y. Takimoto, F. D. Vila, and J. J. Rehr, *J. Chem. Phys.* **127**, 154114 (2007).
- ⁵G. Onida, L. Reining, and A. Rubio, *Rev. Mod. Phys.* **74**, 601 (2002).
- ⁶W. G. Aulbur, L. Jonsson, and J. W. Wilkins, *Solid State Physics*, edited by H. Ehrenreich and F. Spaepen (Academic, New York, 1999), Vol. 54, p. 1.
- ⁷G. Strinati, H. J. Mattausch, and W. Hanke, *Phys. Rev. Lett.* **45**, 290 (1980).
- ⁸E. Luppi, H. Hübener, and V. Vénier, *Phys. Rev. B* **82**, 235201 (2010).
- ⁹E. K. Chang, E. L. Shirley, and Z. H. Levine, *Phys. Rev. B* **65**, 035205 (2001); R. Leitsmann, W. G. Schmidt, P. H. Hahn, and F. Bechstedt, *ibid.* **71**, 195209 (2005); H. Hübener, *Phys. Rev. A* **83**, 062122 (2011).
- ¹⁰David Pines, Leo P. Kadanoff, and Gordon Baym, *Quantum Statistical Mechanics* (Perseus Books, New York, 1994).
- ¹¹S. Schmitt-Rink, D. S. Chemla, and H. Haug, *Phys. Rev. B* **37**, 941 (1988).
- ¹²M. F. Pereira and K. Henneberger, *Phys. Rev. B* **58**, 2064 (1998).
- ¹³K. Henneberger and H. Haug, *Phys. Rev. B* **38**, 9759 (1988).
- ¹⁴K. Hannewald, S. Glutsch, and F. Bechstedt, *Phys. Rev. Lett.* **86**, 2451 (2001).
- ¹⁵H. Khler, N. Kwong, and H. A. Yousif, *Comput. Phys. Commun.* **123**, 123 (1999).
- ¹⁶M. P. Puig von Friesen, C. Verdozzi, and C.-O. Almbladh, *Phys. Rev. Lett.* **103**, 176404 (2009).
- ¹⁷N.-H. Kwong and M. Bonitz, *Phys. Rev. Lett.* **84**, 1768 (2000).
- ¹⁸N. E. Dahlen and R. van Leeuwen, *Phys. Rev. Lett.* **98**, 153004 (2007).
- ¹⁹D. Kremp, M. Schlanger, and W.-D. Kraeft, *Quantum Statistics of Nonideal Plasmas* (Spinger, Berlin, 2004).
- ²⁰W. Schafer and M. Wegener, *Semiconductor Optics and Transport Phenomena: From Fundamentals to Current Topics* (Springer, Berlin, 2002).
- ²¹W. Kohn and L. J. Sham, *Phys. Rev.* **140**, A1133 (1965).
- ²²B. Farid, R. Daling, D. Lenstra, and W. van Haeringen, *Phys. Rev. B* **38**, 7530 (1988).
- ²³C. D. Spataru, L. X. Benedict, and S. G. Louie, *Phys. Rev. B* **69**, 205204 (2004).
- ²⁴A. Marini and R. Del Sole, *Phys. Rev. Lett.* **91**, 176402 (2003).
- ²⁵G. Pal, Y. Pavlyukh, W. Hübner, and H. C. Schneider, *Eur. Phys. J. B* **79**, 327 (2011).
- ²⁶Y. Ma and M. Rohlfing, *Phys. Rev. B* **77**, 115118 (2008).
- ²⁷Here, we assumed that at equilibrium ($U = 0$) the quasiparticle corrections do not modify the Kohn-Sham Fermi distribution.
- ²⁸C. D. Spataru, L. X. Benedict, and S. G. Louie, *Phys. Rev. B* **69**, 205204 (2004).
- ²⁹K. Rzaewski and R. W. Boyd, *J. Mod. Opt.* **51**, 1137 (2004); W. E. Lamb, R. R. Schlicher, and M. O. Scully, *Phys. Rev. A* **36**, 2763 (1987).
- ³⁰K. S. Virk and J. E. Sipe, *Phys. Rev. B* **76**, 035213 (2007).
- ³¹The intraband terms, the ones for $m = n$, can be obtained by using the Berry curvature (Ref. 30). However, in this work, we did not include intraband matrix elements in our calculations. It is known that they do not affect optical properties of semiconductors and insulators within linear regime, and it is not clear yet how much they are relevant beyond linear optics (see Ref. 41 for a discussion). Moreover, notice that even in presence of the scissor operator, the optical matrix elements derived from the commutation relation are not affected at the lowest order by the presence of this additional nonlocal operator (Refs. 8 and 42).
- ³²M. Nekovee, W. M. C. Foulkes, and R. J. Needs, *Phys. Rev. Lett.* **87**, 036401 (2001).
- ³³Note that the response functions, calculated by Eq. (11), as for the standard $G_0W_0 + \text{BSE}$ approach, are not conserving in the Baym-Kadanoff sense (Ref. 10). This is the consequence of the artificial scissor operator and of the dissipative effects introduced by hand, respectively, in Eq. (11) and Sec. III B.
- ³⁴A. Marini, C. Hogan, M. Grüning, and D. Varsano, *Comput. Phys. Commun.* **180**, 1392 (2009).
- ³⁵The DFT calculations for the *h*-BN have been performed using the unitary cell as in Ref. 36, a $8 \times 8 \times 4k$ -point sampling, the local-density approximation for the exchange-correlation functional (Ref. 43), Troullier-Martins pseudopotentials (Ref. 44), and a plane-wave cutoff of 40 Ry. All DFT calculations have been performed with the ABINIT code (Ref. 45). *Ai*-MBPT calculations have been performed using the YAMBO code (Ref. 34). For the G_0W_0 , we used 60 bands to calculate the dielectric constant and to expand the Green's functions. For the dielectric matrix size, we used a cutoff of 2 Ha on the reciprocal lattice vectors and the plasmon-pole model as implemented in the YAMBO code (Ref. 34). For the BSE, we use the same parameter for dielectric constant in the screening and we consider transitions from the two upper valence bands to the two lower conduction bands. The response is calculated along the (0, 1, 0) direction.
- ³⁶L. Wirtz, A. Marini, and A. Rubio, *Phys. Rev. Lett.* **96**, 126104 (2006); L. Wirtz, A. Marini, M. Grüning, C. Attaccalite, G. Kresse, and A. Rubio, *ibid.* **100**, 189701 (2008).
- ³⁷In all the simulations, the time step is 0.5 as. As described in Sec. III B, we introduced an additional term in Eq. (11) to simulate dissipative effects. We chose 1 ns for the lifetime of the perturbed electronic population, and 5 fs for the dephasing rate.
- ³⁸A. V. Kanaev, J.-P. Petitet, L. Museur, V. Marine, V. L. Solozhenko, and V. Zafirooulos, *J. Appl. Phys.* **96**, 4483 (2004).
- ³⁹A. Marini, *Phys. Rev. Lett.* **101**, 106405 (2008).
- ⁴⁰E. Schwegler, M. Challacombe, and M. Head-Gordon, *J. Chem. Phys.* **106**, 9708 (1997); X. Blase, C. Attaccalite, and V. Olevano, *Phys. Rev. B* **83**, 115103 (2011).
- ⁴¹C. Aversa and J. E. Sipe, *Phys. Rev. B* **52**, 14636 (1995).
- ⁴²J. L. Cabellos, B. S. Mendoza, M. A. Escobar, F. Nastos, and J. E. Sipe, *Phys. Rev. B* **80**, 155205 (2009).
- ⁴³D. M. Ceperley and B. J. Alder, *Phys. Rev. Lett.* **45**, 566 (1980).
- ⁴⁴N. Troullier and J. L. Martins, *Phys. Rev. B* **43**, 1993 (1991).
- ⁴⁵X. Gonze, J. M. Beuken, R. Caracas, F. Detraux, M. Fuchs, G. M. Rignanese, L. Sindic, M. Verstraete, G. Zerah, F. Jollet, M. Torrent, A. Roy, M. Mikami, P. Ghosez, J. Y. Raty, and D. C. Allan, *Comput. Mater. Sci.* **25**, 478 (2002).